Available online at www.sciencedirect.com

ScienceDirect

Geochimica et Cosmochimica Acta 179 (2016) 110–122

Geochimica et Cosmochimica Acta

www.elsevier.com/locate/gca

Hydration effects on gypsum dissolution revealed by in situ nanoscale atomic force microscopy observations

A. Burgos-Cara [a], C.V. Putnis [b,c], C. Rodriguez-Navarro [a], E. Ruiz-Agudo [a,*]

[a] Departamento de Mineralogía y Petrología, Universidad de Granada, 18071 Granada, Spain
[b] Institut für Mineralogie, Universität Münster, 48149 Münster, Germany
[c] Nanochemistry Research Institute, Department of Chemistry, Curtin University, Perth 6845, Australia

Received 19 June 2015; accepted in revised form 5 February 2016; Available online 11 February 2016

Abstract

Recent work has suggested that the rates of mineral dissolution in aqueous solutions are dependent on the kinetics of dehydration of the ions building the crystal. Dehydration kinetics will be ultimately determined by the competition between ion–water and water–water interactions, which can be significantly modified by the presence of background ions in solution. At low ionic strength, the effect of electrolytes on ion–water (electrostatic) interactions will dominate (Kowacz et al., 2007). By performing macroscopic and in situ, microscopic (atomic force microscopy) dissolution experiments, the effect of background electrolytes on the dissolution kinetics of gypsum ($CaSO_4{\cdot}2H_2O$) {0 1 0} cleavage surfaces is tested at constant, low ionic strength (IS = 0.05) and undersaturation (saturation index, SI = −0.045). Dissolution rates are systematically lower in the presence of 1:1 background electrolytes than in an electrolyte-free solution, regardless of the nature of the electrolyte tested. We hypothesize that stabilization of the hydration shell of calcium by the presence of background ions can explain this result, based on the observed correlations in dissolution rates with the ionic surface tension increment of the background ion in solution. Stabilization of the cation hydration shell should favor dissolution. However, in the case of strongly hydrated ions such as Ca^{2+}, this has a direct entropic effect that reduces the overall ΔG of the system, so that dissolution is energetically less favorable. Overall, these results provide new evidence that supports cation dehydration being the rate-controlling step for gypsum dissolution, as proposed for other minerals such as barite, dolomite and calcite.

1. INTRODUCTION

Knowledge of the dissolution behavior of gypsum ($CaSO_4{\cdot}2H_2O$) in aqueous solutions is of primary importance in many natural and technological processes. The study of the mechanisms and kinetics of water–gypsum interactions may provide insights into the role of gypsum on crustal deformation in numerous geological settings and in trapping large oil and gas accumulations (De Meer and Spiers, 1997). A quantitative, mechanistic-based understanding of gypsum behavior in contact with aqueous solutions is also relevant for predicting the evolution of the wide areas of gypsum karsts existing worldwide, their instability and potential collapse (Jeschke et al., 2001).

Additionally, the dissolution of gypsum has important environmental implications. The presence of calcium and sulfate ions in water influences the dissolution of other minerals containing toxic metals (e.g. uranium) (Kuechler et al., 2004) and the quality of drinking water (Raines and Dewers, 1997). Moreover, it can help to ameliorate the acidity of soils as it permits the complete precipitation of dissolved aluminum and increases the level of dissolved calcium in the soil solution allowing roots to penetrate into the subsoil (Sumner et al., 1986).

* Corresponding author.
E-mail address: encaruiz@ugr.es (E. Ruiz-Agudo).

http://dx.doi.org/10.1016/j.gca.2016.02.008
0016-7037/

An in-depth understanding of gypsum dissolution behavior is also required in the oil and gas industry, as gypsum is one of the main inorganic scale deposits in hydrocarbon reservoirs (Raju and Atkinson, 1990), which can significantly affect oil recovery. Enhanced chemical dissolution of gypsum precipitates is an efficient way to remove these scales. A better understanding of gypsum dissolution would also provide insights into the mechanism of the strong enhancement of creep of plasterboards in humid environments. It has been suggested that this behavior is related to the dissolution of gypsum in the intercrystalline water of the plaster. To slow down such a process, anti-creep salts are commonly added (Pachon-Rodriguez et al., 2011). Knowledge of the dissolution kinetics of gypsum in water containing different electrolytes is thus necessary to find new additives to avoid such a problem. Finally, gypsum dissolution plays a critical role in the hydration of Portland cement. Gypsum is added to suppress the rapid hydration reaction of calcium aluminate during cement setting. Immediately upon wetting of the cement, the dissolution of gypsum releases calcium and sulfate ions into solution that react with aluminate and hydroxyl ions forming ettringite ($Ca_6Al_2(SO_4)_3(OH)_{12}\cdot 26H_2O$) needles, which subsequently precipitate on calcium aluminate grains, retarding their hydration (Chen and Jiang, 2009).

Most commonly, water in contact with rock-forming minerals or technologically relevant materials contains significant and variable amounts of ions in solution. In all the applications described above, the morphology and rates of gypsum dissolution can be affected by the presence of ions in solution in an, as yet, unknown way. Few studies have dealt with the effect of electrolytes on gypsum reactivity. Brandse et al. (1977) found that sodium chloride significantly increased the gypsum growth rate. Traditionally, the effect of foreign ions on mineral growth or dissolution behavior has been ascribed to changes (increase) in solubility (ionic strength effect, Buhmann and Dreybrodt, 1987) or to the ability of some ions to adsorb at the mineral surface and hinder the detachment of the ions building the crystal. However, current research suggests that the control that background electrolytes exert on water structure is limited to the local environment surrounding the ions and is not related to long-range electric fields emanating from the ions, nor with the specific interactions with active sites on mineral surfaces (e.g. Kowacz and Putnis, 2008; Ruiz-Agudo et al., 2010, 2011a,b). In this sense, the early work by Brandse et al. (1977) showed an enhancement in gypsum growth kinetics above the expected increase associated with the relative increase in the solubility of gypsum in brines. Bosbach et al. (1996) concluded that the interaction between gypsum (0 1 0) surfaces and water at such interfaces determines the kinetics of growth in the presence of background electrolytes. In particular, these authors propose an increased dehydration frequency for hydrated Ca^{2+} in the presence of Cl^- relative to NO_3^-. Interestingly these authors indicate that such a hydration effect cannot be deciphered from bulk growth experiments, and in situ microscale experiments are needed. Similar effects should thus be expected during dissolution experiments. The effect of foreign ions on the hydration shell(s) of the building units of the crystal and the ions' capacity to break or structure water (i.e. chaotropic and kosmotropic ions, respectively) seem to strongly dictate the influence that these background ions have on the kinetics of mineral growth and dissolution (Kowacz and Putnis, 2008; Ruiz-Agudo et al., 2010, 2011a,b).

Several authors have studied gypsum reactivity – dissolution and growth – by in situ, microscopic techniques including atomic force microscopy (AFM) and scanning force microscopy (SFM) (Bosbach and Rammensee, 1994; Bosbach et al., 1996; Hall and Cullen, 1996; Fan and Teng, 2007); however, none of them have considered the effect of specific background ions on the kinetics of gypsum dissolution. Here we report the results of a systematic study on the effect of a series of 1:1 background electrolytes (Na-bearing and Cl-bearing salts) on the kinetics of dissolution of gypsum (0 1 0) cleaved surfaces. Experiments were performed under conditions of low ionic strength, when the effects of background ions on the hydration shell of the ions building the crystal are thought to dominate (e.g. Ruiz-Agudo et al., 2011b). This study was carried out by combining in situ nanoscale dissolution experiments by means of AFM that allows direct observations and quantification of the kinetics of the processes occurring at the mineral surfaces, with macroscopic flow-through dissolution experiments. We show that dissolution rates are systematically lower in the presence of low concentrations of background salts compared to electrolyte-free solutions, regardless of the nature of the electrolyte tested. Dissolution rates under the conditions of our experiments correlate directly with ionic radius and inversely with the differences, between the two ions that compose a background salt, of the diffusion coefficients. These trends are explained considering the differential stabilization of hydration shells of calcium ions achieved in the presence of each of the salts.

2. METHODOLOGY

2.1. Materials

Freshly cleaved gypsum {0 1 0} surfaces (pure crystals from Naica, Chihuahua, Mexico) were used for all flow-through dissolution experiments. In the case of AFM experiments, crystals of ca. 3 × 3 × 1 mm in size were used as substrates. For the macroscopic experiments, disk-shaped crystals of ca. 14 mm in diameter and 2 mm thick were used. The disk samples used for bulk experiments were cleaved from a cylindrical core, whose bases are parallel to the (0 1 0) cleavage plane. This core was previously obtained from a centimeter-sized gypsum crystal using a cylindrical drill. Then, fragments were obtained by cleaving the crystals perpendicularly to the elongation axis of the cylinder.

Five 1 M saline stock solutions (NaCl, NaBr, $NaNO_3$, KCl, CsCl and NH_4Cl) were prepared from high purity reagent grade reactants (Sigma Aldrich) using doubly-deionized water type I+ (<18.2 MΩ). A saturated $CaSO_4$ stock solution was also prepared by dissolving gypsum powder in excess (obtained by milling the same gypsum crystals used in dissolution experiments) in water type I+

Table 1
Composition of solutions used in the dissolution experiments.

Background ion	Total ionic strength (IS) (25.5 °C)	Saturation index with respect to gypsum, SI (25.5 °C)	Background electrolyte concentration (mM)
NaCl	0.050	−0.046	4.59
KCl	0.050	−0.046	5.24
CsCl	0.050	−0.045	3.30
NaBr	0.050	−0.046	4.59
$NaNO_3$	0.050	−0.046	4.59
NH_4Cl	0.050	−0.046	7.01

and allowing it to equilibrate at room temperature (21.5 ± 0.2 °C) overnight. Subsequently, the solution was vacuum filtered by using 0.22 μm Millipore membranes. Solutions were clear of solids as shown by the absence of Tyndall effect when a laser was directed to the solutions after filtering. This was further confirmed by measurements of the transmittance of the solution using an Optrode probe. Working solutions were prepared by mixing measured proportions of the saturated gypsum stock solution, the corresponding saline stock solution and water type I +. The composition of the solutions used in flow-through dissolution experiments is listed in Table 1. The composition was designed using PHREEQC software (version 3.1.1-8288) and the PHREEQC.dat database for a fixed ionic strength (IS) of 0.050 ± 0.005 and a saturation index with respect to gypsum (SI) of −0.045 ± 0.003. The ionic strength of a salt solution is defined as: $IS = 0.5 * (\Sigma_i\ c_i\ z_i^2)$, where c_i is the concentration of each ion and z_i is the charge on each ion. The saturation index can be estimated as: $SI = \log((a_{Ca}^{2+} \cdot a_{SO4}^{2-})/K_{sp}$, where a_{Ca}^{2+} and a_{SO4}^{2-} are the activities of calcium and sulfate ions and K_{sp} is the solubility product of gypsum at the given temperature (PHREEQC.dat 3.1.1-8288).

2.2. In situ AFM flow-through dissolution experiments

AFM flow-through dissolution experiments on gypsum {0 1 0} surfaces were carried out using a Digital Instruments (Bruker) Nanoscope III Multimode, equipped with a fluid cell. Observations were performed in contact mode at ambient temperature (21.5 ± 0.2 °C) assuming a temperature increase inside the cell of 4 °C due to laser heating according to data estimated by Bruker for the operating conditions. Solution flow was controlled by syringe injections after every image acquired without disengaging the tip from the surface (effective flow rate ca. 85 mL h^{-1}). AFM images were collected at a scanning frequency of 4 Hz using Si_3N_4 tips with a 45 nm coating of Ti/Au (Bruker, tip model SNL-10) and analyzed with Nanoscope software (Version 1.40). Before each AFM dissolution experiment, a saturated gypsum solution at room temperature (21.5 ± 0.2 °C) was passed over the crystal to clean the cleaved surface, as well as to adjust the AFM parameters.

Measurements of step retreat velocity (or etch pit spreading rate) were made from sequential images scanned in the same direction. All etch pits in several 5 × 5 μm scanned areas were monitored; moreover, at least 2 replicates of all the experiments were performed. The lower number of measurement for each background salt (N) is always greater than 40, being in some cases up to 200. The uncertainty of the measurements is reported as $2\sigma_N$ $\left(\sigma_N = \frac{\sigma_{N-1}}{\sqrt{N}}\right)$. When needed, error propagation was done according to direct derivative criteria. The etch pit spreading rate v_i was calculated by measuring the length increase per unit time between opposite parallel steps in sequential images, with $i = a$ for the [0 0 1] direction and $i = b$ for the [1 0 1] direction. During dissolution, etch pits deepen and widen, thus changing their height and lateral dimensions. To take into account the geometric changes that take place on the crystal surface, we used volumetric acceleration per height, a_v/h, which is time-independent and only depends on the etch pit spreading rates in a and b directions. This parameter describes how fast the surface area of an etch pit spreads with time (valid also for island spreading and growth processes) and gives a better approximation of the kinetics of volume loss during dissolution than considering only the spreading rate along a single crystallographic direction. It is defined according to (see Appendix 1 for further details and explanation):

$$a_V/h = \frac{d^2V}{h \cdot dt^2} = 2 \cdot \sin(\alpha) \cdot v_a \cdot v_b \quad (1)$$

where a and b are the length of the etch pits measured by AFM, v_a and v_b the calculates etch pits retreat velocities, h the height of the etch pits, α the angle between the directions [0 0 1] (a) and [1 0 1] (b) and V the empty volume of the etch pits.

Overall dissolution rates, $R_{\text{Total Calcium}}$ (mmol m^{-2} s^{-1}), could thus be simply estimated by multiplying the volumetric acceleration, a_v, by the etch pit density expressed in terms of fractional area occupied by etch pits. Indeed, earlier works (e.g. Jordan and Rammensee, 1998) have calculated overall dissolution rates using a similar approach, but considering as a simplification that the walls of the etch pits are perpendicular to the bottom of the pits. However, within the same substrate, the etch pit density (related to the defect density of the material) may vary significantly. Moreover, both the defect and etch pit density can vary significantly between gypsum substrates from different locations, thus making a comparison between different experiments complicated. This is not very important in the case of calcite or dolomite, where the high etch pit density in the scanned area (typically 3 × 3 μm up to 10 × 10 μm) leads to highly reproducible values of etch pit densities and thus overall dissolution rates.

However, the main issue with the gypsum used in our experiments under the experimental conditions selected, is the very low etch pit density (which varies from none up to three-four etch pits) in the scanned area accessible with the scanner used in our experiments. This can lead to variations in overall rates values determined using the approach described above, similar to that used for carbonates under far from equilibrium conditions, of up to 400%. Therefore, microscopically derived spreading rate data cannot be accurately translated into bulk dissolution rates by assuming an average defect density, as was also found by Bosbach et al. (1996) for gypsum growth. This is why we decided to use just the volumetric acceleration, a parameter that is independent of etch pit density but somehow reflects the volume release to the solution, and it is closely related to absolute dissolution rate.

Additionally, 6 mL aliquots of the output solution were collected after flowing through the AFM fluid cell for subsequent Ca^{2+} analysis by inductively coupled plasma optical emission spectrometry (ICP-OES, Varian Vista proaxial). From these measurements, macroscopic dissolution rates of gypsum, $R_{\text{Total Calcium}}$ (mmol cm^{-2} s^{-1}) were calculated as follows:

$$R_{\text{Total Ca}} = \frac{Ca_T \cdot Q}{A} \quad (2)$$

where Ca_T the total calcium in the effluent solution minus the influent calcium (mmol L^{-1}) determined by ICP-OES, Q is the solution flow rate (L s^{-1}) and A is the geometric area of calcite exposed to the solution (m^2).

2.3. Macroscopic flow-through dissolution experiments

For the macroscopic experiments the crystals were fixed to the bottom of an opened Teflon® reactor with nanocarbon dispersion (Leit-C, Plano GMBH). Solutions were allowed to flow continuously (1 mL min^{-1}) for 90 min using a peristaltic pump (Miniplus Evolution, Gilson, Inc.). In-line measurements of pH and free-Ca^{2+} were performed during the experiment at different heights from the crystal surface using a pH micro-electrode (PHR-146 Micro Combination pH Electrode, Lazar Research Laboratories, Inc.) and a Ca^{2+} ion-selective microprobe (LIS-146 CACM Micro Calcium Ion Electrode, Lazar Research Laboratories, Inc.). A mechanical step-displacement micrometer (Model 9664-0107, Limit, Sweden) was used to set the height of the microprobes. Fig. 1 shows a schematic representation of the experimental set-up. The response time of the pH electrode is 1 s, and the time in each position (total number of positions = 6) was 10 s. Therefore, at the time in which the reading was recorded, the probe had had enough time to settle in the corresponding position, reporting a constant value. Measurements in each point were carried out every 60 s. Once the data were collected, going up and down in distance from the mineral surface with the time, the plot was constructed by interpolation of the information between measured points.

Experiments were performed at constant room T (22 ± 1 °C). Additionally, 5 mL aliquots of the output solution were collected at different t intervals and analyzed for total calcium by ICP-OES (Varian Vista proaxial). From these measurements, macroscopic dissolution rates of gypsum, $R_{\text{Total Ca}}$ (mmol m^{-2} s^{-1}) were calculated using also the Eq. (2).

3. RESULTS

3.1. Dissolution of {0 1 0} gypsum surfaces as seen by AFM

Freshly cleaved {0 1 0} gypsum surfaces seen in air show atomically flat terraces (Fig. 2a). To induce dissolution, samples were brought into contact with calcium sulfate solutions that were initially saturated with respect to gypsum at 21.5 °C. Upon injection of the solutions in the fluid cell, laser heating increases the solution T up to 25.5 °C. As gypsum solubility increases with T, the solutions become undersaturated with respect to gypsum (SI = −0.045) and dissolution of gypsum surfaces begins as reflected by the immediate formation and spreading of elongated etch pits (Fig. 2b–h). These conditions were chosen to maintain a level of surface reactivity so that changes occurring between successive scans could be easily monitored and measured using AFM.

The edges of the etch pits show a typical height of ~11 Å (Fig. 3b and cross-section). Etch pit edges are aligned parallel to two main directions ([0 0 1] and [1 0 1]) and dissolution progresses by retreat of these edges. The step retreat velocity is constant over the course of an experiment (20–40 min) but differs significantly for the two main directions. For example, in the case of dissolution in the absence of any background electrolyte (see Fig. 2), the velocity of the faster moving step is 6.6 ± 0.2 nm/s, while that of the slower moving step is 0.7 ± 0.1 nm/s. In our experiments, the slow-moving edges of the etch pits are parallel to ⟨0 0 1⟩, while the faster moving edges are parallel to ⟨1 0 1⟩, as shown in Fig. 3c. No significant changes in etch pit morphology or dissolution mechanism were observed in the presence of the 1:1 background electrolytes tested here. However, etch pit spreading rates (v_a and v_b) and the volumetric acceleration per unit height (a_v/h) determined from measurements of length changes in consecutive AFM images varied systematically depending on the nature of the salt used to adjust the ionic strength (Table 2 and Fig. 4).

3.2. Dissolution rates, calcium concentration and pH profiles determined in macroscopic flow-through experiments

Strong mm-scale concentrations gradients are typically formed during gypsum dissolution under unstirred conditions (Colombani and Bert, 2007). However, measurements performed using ion selective microelectrodes at different heights from the mineral surface show that under the conditions of continuous flow of our experiments there is almost no concentration gradient from the mineral surface towards the bulk, particularly ca. 1750 s after the beginning of the experiments, when the steady state has been reached in the system (see Appendix 2). Rates calculated from the free-Ca (determined using the ion-selective microelectrode) and total calcium (determined by ICP-OES) concentration

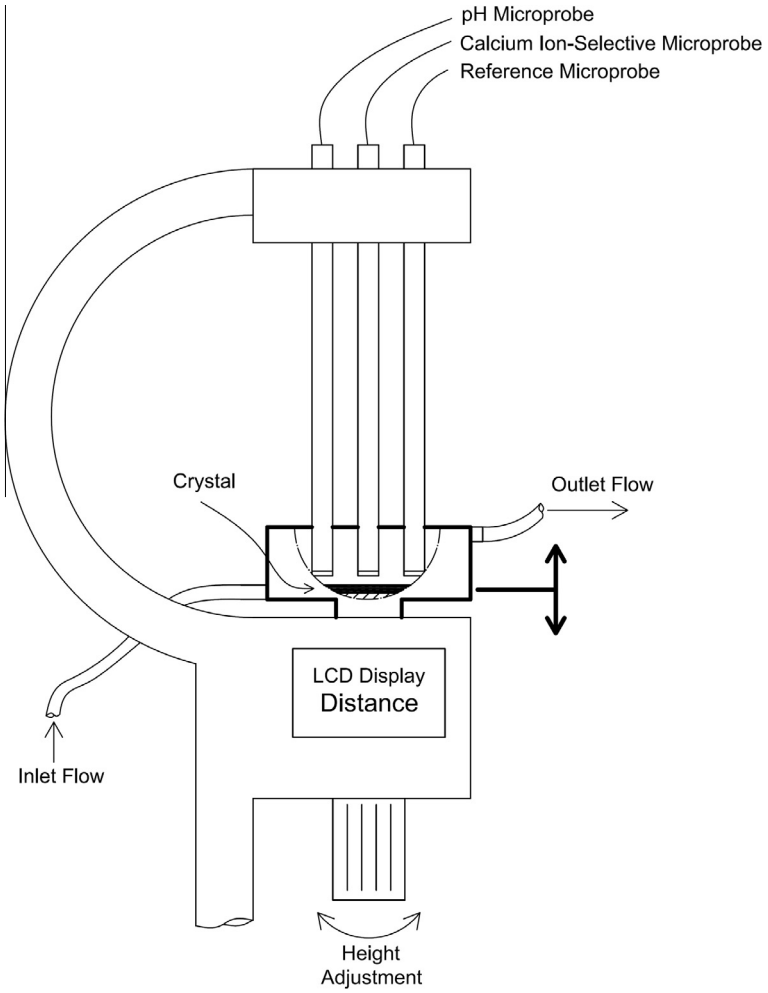

Fig. 1. Experimental set up for the position-sensitive measurements of free-Ca concentration and pH using microelectrodes.

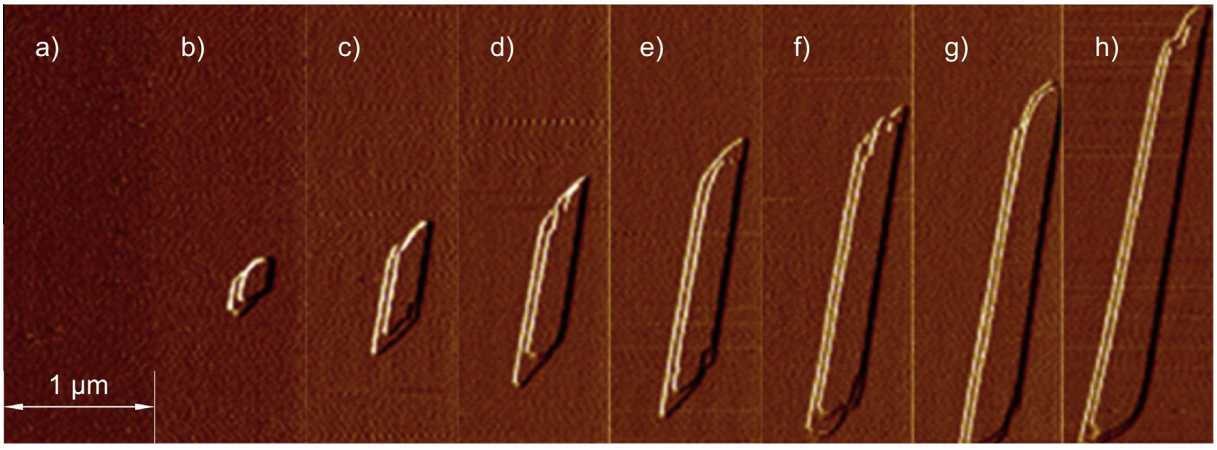

Fig. 2. AFM deflection images of a gypsum (0 1 0) cleaved surface exposed to an undersaturated solution (SI = −0.045) for increasing periods of time (time lapse between images ca. 85 s). Background electrolyte: NaCl (IS = 0.05).

measurements at steady state depend on the background electrolyte present in the solution, as shown in Table 3 and Fig. 5.

AFM-derived parameters (etch pit spreading rates and the volumetric acceleration per unit height) are regarded to be more accurate and representative of the actual

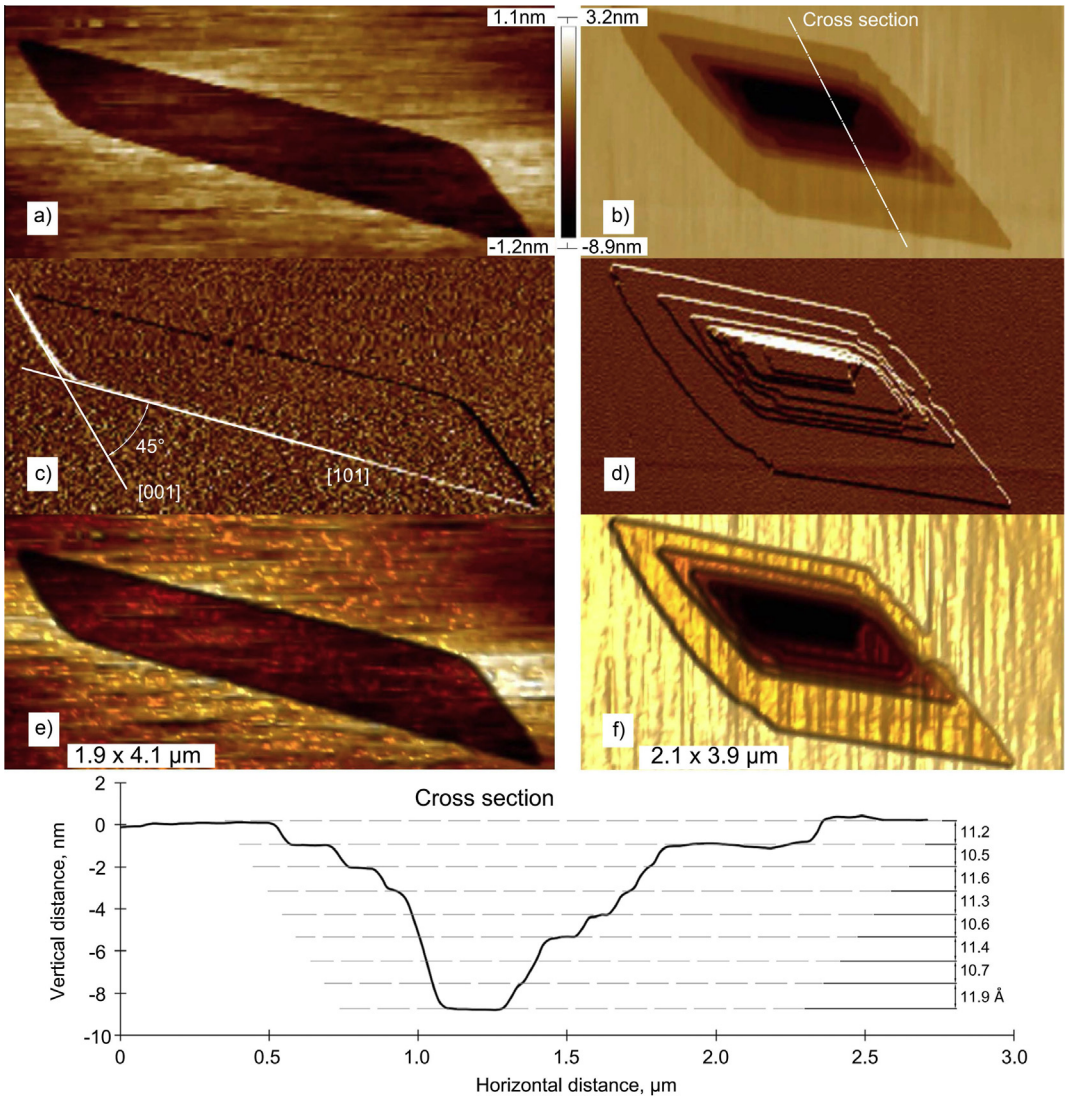

Fig. 3. AFM (a and b) height, (c and d) deflection and (e and f) 3D images of (a, c, and e) monolayer and (b, d, and f) multiple layer etch pits formed on gypsum (0 1 0) cleaved surfaces exposed to an undersaturated solution (SI = −0.045). Background electrolyte: NaCl (IS = 0.05).

dissolution rates, than rates determined from ion concentrations in the solutions after contact with the solid. A critical issue is the use of geometric surface area instead of the actual reactive surface area. Determining the actual reactive surface area is not an easy task. Recent studies have shown that surface topography plays a major role in determining dissolution kinetics and mechanisms. Experimental studies performed using in situ, nanoscale imaging techniques such as AFM or VSI have shown that even for the same mineral surface, different sites may have different reactivity (Fischer et al., 2012; Luttge et al., 2013).

Therefore, our work suggests that a more adequate approach for a comparative study on the effects of background electrolytes on mineral dissolution kinetics, which would remove the uncertainty related to actual reactive surface area, could be the evaluation of dissolution rates from observations and measurements of dissolving surfaces, such as those reported in this paper. However, note that overall rates determined from measurements of ion concentrations in AFM and macroscopic dissolution experiments show (roughly) comparable trends with different background electrolytes to those seen for AFM-derived parameters. Nevertheless, problems related to uncertainties in the actual reactive surface area described above precludes making any conclusion on these data, confirming that AFM-derived parameters are more accurate for interpreting trends in dissolution rates.

4. DISCUSSION

4.1. Dissolution features and gypsum crystal structure

Nanoscale observations of mineral surfaces during dissolution have shown that etch pit formation is a fundamental step in this process, as it provides a source of step edges where kink site nucleation is energetically favored in

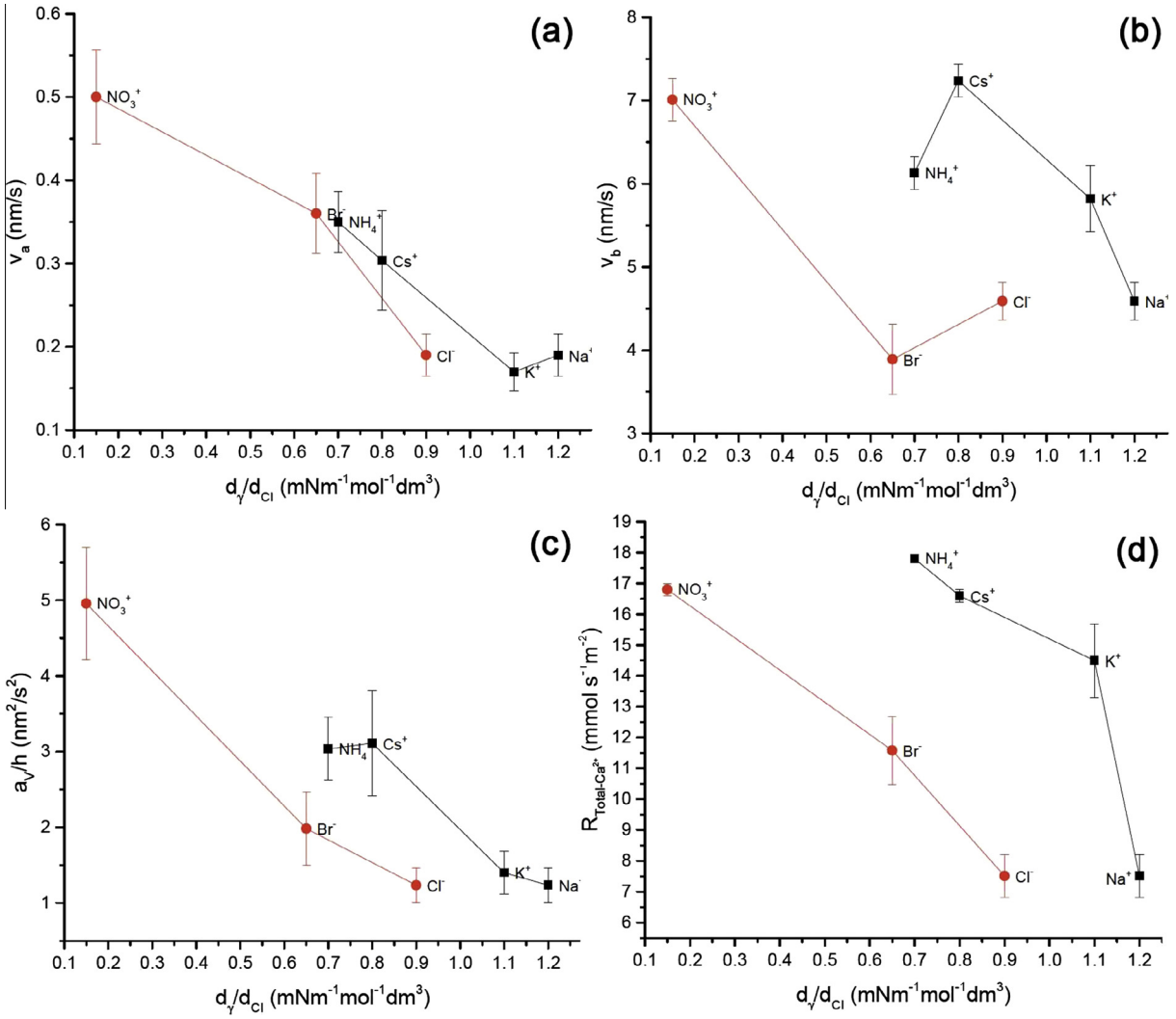

Fig. 4. Etch pit spreading rates (v_a and v_b, nm s^{-1}), volumetric acceleration (a_V/h, nm^2 s^{-2}) and overall dissolution rates ($R_{\text{total Ca}}$, mmol s^{-1} m^{-2}, determined from calcium measurements in the solutions using ICP-OES, see the text for further explanation) on gypsum cleavage surfaces for the different background electrolytes used in this study, represented as a function of the ionic surface tension increment of the background ion, $k_i = d\gamma/d_{Cl}$. Error bars show $2\sigma_N$ of the measurements.

comparison to a flat surface (Ruiz-Agudo and Putnis, 2012 and references therein). In this study, etch pits form on gypsum surfaces immediately upon injection of the undersaturated solutions in the fluid cell. Deep, multiple-layer etch pits are commonly observed under the conditions selected for this study. As described for other minerals such as calcite (e.g. Liang et al., 1996), these etch pits nucleate at surface defects, most likely at dislocations. Shallow, single-layer steps are not frequently found. Note that the formation of these steps that nucleate at point defect or defect-free areas typically requires a high degree of undersaturation and our experiments are performed at close to equilibrium conditions.

The gypsum structure can be described as a regular stacking of double layers of calcium and sulfate ions perpendicular to the [010] direction, each of them separated by a double layer of water molecules (Fig. 6). Along the [010] direction, the unit cell is globally formed by two of these calcium-sulfate double layers (Fig. 6). The observed deep, etch pits represent a source of steps that propagate with the progress of the dissolution process, each with a height of approximately 2/3 of the (010) d-spacing. This corresponds to the height of one and a half calcium-sulfate double layers separated by a double layer of water molecules (10.5 Å) that corresponds to the average height measured from AFM images of etch pits (~11 Å) (Fig. 3). During gypsum dissolution, steps parallel to ⟨001⟩ retreat at slower rates than steps parallel to ⟨101⟩. As explained by Hall and Cullen (1996), this observation is consistent with the trend in crystal face stability described for gypsum. In gypsum the most stable faces are (010) and (120), while (011) and (111) are fast growing and less stable (Weijnen et al., 1987). The ⟨001⟩ steps are at the intersection of the (010) plane with the stable (120) plane, which we observe to be very slow moving and stable during dissolution. On the other hand, the ⟨101⟩ steps are the intersection of the (010) plane and the unstable (111) plane. Under the conditions tested here, dissolution occurs preferentially along

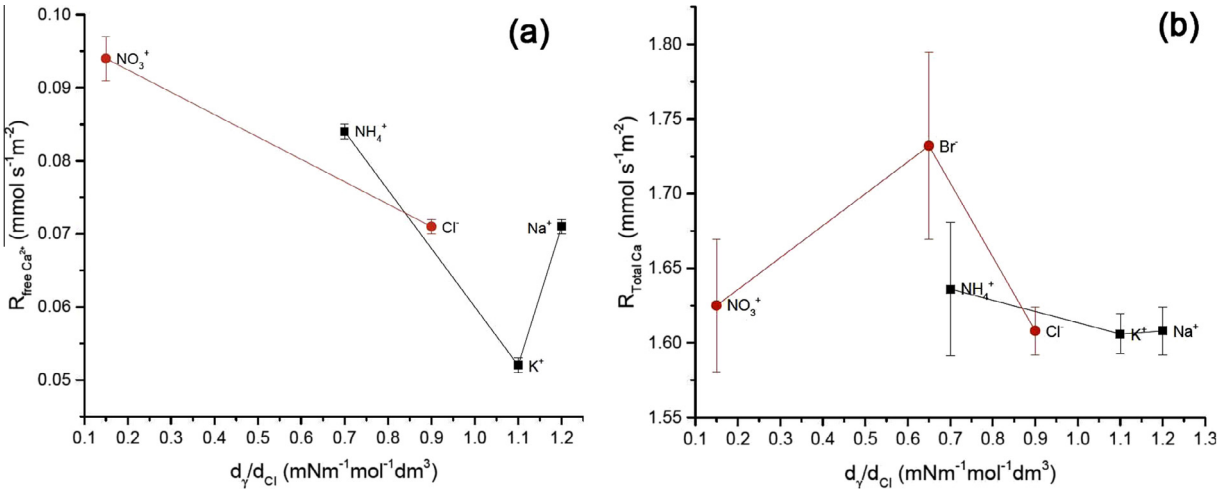

Fig. 5. Dissolution rates determined in macroscopic, flow-through dissolution experiments from measurements of free Ca^{2+} concentration ($R_{free\text{-}Ca2+}$, mmol s^{-1} m^{-2}, determined from free calcium measurements in the solutions using ion selective microelectrodes, see the text for further explanation) and total calcium ($R_{total\ Ca}$, mmol s^{-1} m^{-2}, determined from calcium measurements in the solutions using ICP-OES, see the text for further explanation) on gypsum cleavage surfaces for the different background electrolytes used in this study represented as a function of the ionic surface tension increment of the background ion, $k_i = d\gamma/d_{Cl}$. Error bars show $2\sigma_N$ of the measurements.

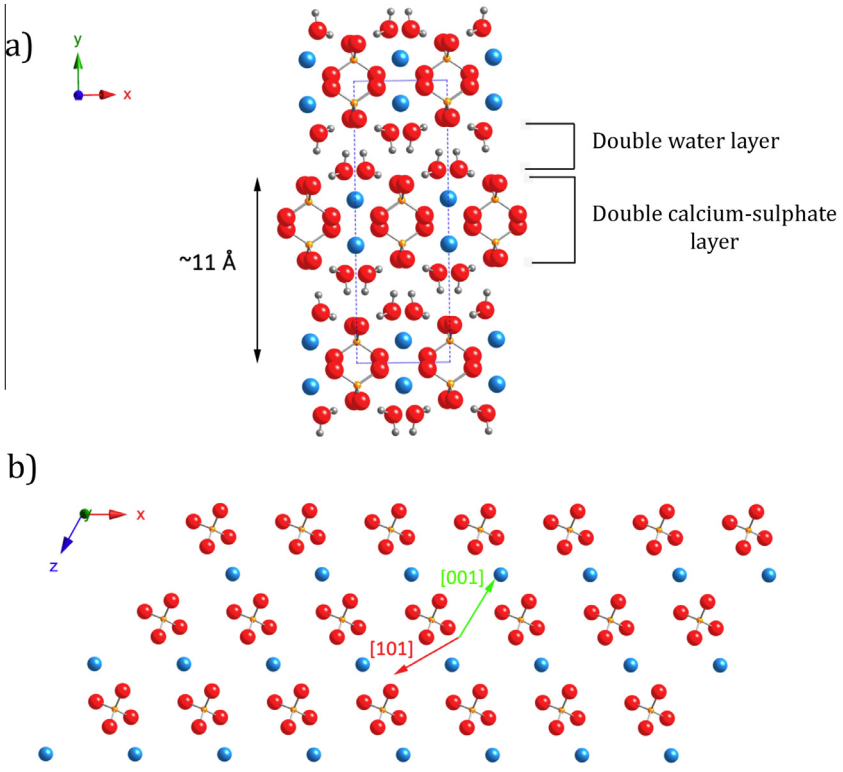

Fig. 6. (a) Sketch showing the structure of gypsum, view perpendicular to the (0 0 1) plane. The unit cell is marked by a discontinuous, blue line. (b) Normal view of the atomic arrangements in the (0 1 0) plane of gypsum. Color code: calcium (blue), sulfur (orange), oxygen (red), hydrogen (gray). (For interpretation of the references to color in this figure legend, the reader is referred to the web version of this article.)

these steps, which spread significantly faster than the ⟨0 0 1⟩ steps. Furthermore, the observation of such a strong degree of crystallographic control on step spreading indicates that gypsum dissolution is controlled by the rate of detachment of the ions building the crystal and not by diffusion towards the bulk solution under the compositional and flow conditions used in this study (Hall and Cullen, 1996). Despite the fact that concentration gradients develop at the gypsum-solution interface, as shown by free-Ca and pH measurements using microelectrodes, the rate of ion detachment from the gypsum surface seems to be exclusively determined by structural factors.

4.2. Dissolution at low ionic strength: stabilization of Ca^{2+} hydration shells by background electrolytes

Step edges on a mineral surface in contact with a solution are not static even at equilibrium; ions building the crystal are constantly attaching and detaching from/into solution (De Yoreo and Vekilov, 2003). Dissolution from an undersaturated solution occurs because the flux of molecules detaching from the crystal surface exceeds the flux of molecules attaching to the surface. The overall rate of the process is given by the difference between the kinetics of the attachment and detachment processes at step edges, which are determined by the energy barriers seen by the molecules (De Yoreo and Vekilov, 2003). Different experimental studies over the last decades have shown that rates of mineral growth and dissolution are ultimately controlled by the kinetics of hydration/dehydration of the ions building the crystal (Dove and Czank, 1995; Pokrovsky and Schott, 2002; Kowacz et al., 2007; Kowacz and Putnis, 2008; Ruiz-Agudo et al., 2010, 2011a,b). In particular, Kowacz et al. (2007) showed that the growth rate of barite exhibits a maximum for a lattice ion ratio in solution (r) when barium activity exceeded that of sulfate, implying a lower attachment frequency factor for barium than for sulfate ions. Indeed, lowering the solvation of the barium ion by the addition of methanol to the growth solution resulted in a maximum growth rate occurring at $r = 1$, as would be expected for equal attachment frequency factors for both building units. Overall, these observations imply that differences in integration rates of the cation and anion in water solutions arise mainly from the difference in their dehydration frequencies, this ultimately being the rate-controlling step during dissolution in stoichiometric solutions.

Over the last decade, a range of independent experiments has shown that the rate at which carbonate crystals grow display a similar dependence on the ion activity ratio, i.e. the solution stoichiometry (e.g. Perdikouri et al., 2009; Stack and Grantham, 2010; Bracco et al., 2012; Wolthers et al., 2012; Bracco et al., 2014). Moreover, our latest experimental results demonstrate as well that calcite dissolution depends on the solution stoichiometry, with dissolution rates reaching a maximum when calcium activity is in excess with respect to stoichiometric conditions (Wolthers et al., 2015).

Based on these previous studies, we assume that in the case of gypsum calcium solvation/desolvation frequency will control as well the rate of cation attachment/detachment to the mineral surface, and thus the kinetics of dissolution under stoichiometric solutions. This will be determined by a competition between building ion–water (electrostatic) and water–water (hydration forces) interactions, which can be significantly modified by the presence of background ions in solution (Kowacz and Putnis, 2008; Ruiz-Agudo et al., 2010, 2011a,b). The effect of background ions on building ion–water interactions is more important in dilute electrolyte solutions, while their effect on water–water interactions seems to be stronger with increasing electrolyte concentration.

According to this model, at the low IS used in our experiments, the dissolution kinetics of gypsum and its dependence on the background electrolyte used to fix the ionic strength could be interpreted considering the specific effects that each of these salts have on the hydration of the building units of the crystal. First, it should be considered that the water molecules in the solvation shell of a solute ion are stabilized by the presence of background counter-ions in the solution (Samoilov, 1967a,b, 1971). This occurs regardless of the counter-ion because there would be a stronger electrostatic interaction between an ion building the crystal and the water molecules surrounding this ion in a dilute electrolyte solution than in pure water (Kowacz and Putnis, 2008; Ruiz-Agudo et al., 2010, 2011a,b).

One could in principle think that stabilization of the cation hydration shell will favor dissolution. The increased affinity of the water molecules to the solute ions in dilute saline solutions, however, hampers dissolution in the case of strongly hydrated ions such as Ca^{2+} or Mg^{2+} compared to weakly-hydrated ions such as Ba^{2+}, as inferred from the values of the free energy of hydration, −1820, −1943 and −1238 kJ mol^{-1} for Mg^{2+}, Ca^{2+} and Ba^{2+}, respectively (Schmid et al., 2000). This is related to the structuring effect of the water molecules when they are ordered around strongly hydrated calcium and magnesium ions. This effect is negative from an entropic point of view (i.e. the presence of strongly hydrated ions in solution upon mineral dissolution increases to some extent the order of the system), and it is augmented by the stabilization of the hydration shell of water molecules around solute ions due to the presence of background salts, thus making the overall dissolution process less energetically favorable (Ruiz-Agudo et al., 2010, 2011a,b). Such an effect is clearly observed in our dissolution experiments. At a constant degree of undersaturation (SI ≈ −0.045) of the solution with respect to gypsum, dissolution rates determined from AFM and macroscopic

Table 2
Etch pit spreading rates (v_a and v_b, nm s^{-1}), volumetric acceleration (a_V/h, nm^2 s^{-2}) and overall dissolution rates ($R_{Total\text{-}Ca}$, mmol s^{-1} m^{-2}, determined from calcium measurements in the solutions using ICP-OES, see the text for further explanation) on gypsum cleavage surfaces for the different background electrolytes used in this study.

	v_a nm/s	2σ	v_b nm/s	2σ	a_v/h nm^2/s^2	2σ	$R_{Total\text{-}Ca}$ mmol s^{-1} m^{-2}	2σ
H_2O	0.74	0.11	6.58	0.11	6.89	0.15	16.1	0.2
NaCl	0.19	0.03	4.59	0.23	1.23	0.23	7.5	0.7
KCl	0.17	0.02	5.82	0.40	1.40	0.28	14.5	1.2
CsCl	0.31	0.06	7.24	0.20	3.11	0.70	16.6	0.2
NH_4Cl	0.35	0.04	6.13	0.20	3.03	0.42	17.8	0.1
NaBr	0.36	0.05	3.89	0.43	1.98	0.48	11.6	1.1
$NaNO_3$	0.50	0.06	7.01	0.26	4.96	0.74	16.8	0.2

Table 3
Dissolution rates determined in macroscopic, flow-through dissolution experiments from measurements of free-Ca concentration ($R_{free\text{-}Ca2+}$, mmol s^{-1} m^{-2}, determined using ion selective microelectrodes, see the text for further explanation) and total calcium ($R_{total\ Ca}$, mmol s^{-1} m^{-2}, determined from calcium measurements in the solutions using ICP-OES, see the text for further explanation) on gypsum cleavage surfaces for the different background electrolytes used in this study.

	$R_{free\text{-}Ca}$[a] mmol s^{-1} m^{-2}	2σ	$R_{Total\text{-}Ca}$ mmol s^{-1} m^{-2}	2σ
H_2O	0.103	0.001	–	–
NaCl	0.071	0.001	1.608	0.0161
KCl	0.052	0.001	1.606	0.01342
NH_4Cl	0.084	0.001	1.636	0.04472
NaBr	–	–	1.732	0.06261
$NaNO_3$	0.094	0.003	1.625	0.04472

[a] Values at steady-state measured using microprobes.

experiments in the presence of the different 1:1 electrolytes used here are systematically lower than those measured in the electrolyte-free solution (see Tables 2 and 3).

4.3. Ion-specific effects on the kinetics of gypsum dissolution

As stated above, electrostatic interactions between background ions and the water in the solvation shell of the calcium ions will ultimately dictate the effect of the background electrolytes on the kinetics of gypsum dissolution in the dilute 1:1 electrolyte solutions used in this study. These electrostatic interactions will be stronger with *decreasing ionic radius* of the background ion (i.e. with decreasing distance between the water dipoles and the unlike electric field of background ions), and thus higher stabilization of water molecules in the solvation shell of the ions building the crystal would occur in the presence of smaller background ions. This would result in decreased dissolution rate in this latter case compared to the case in which bigger background ions are present.

Accordingly, changes in *the effective charge of the electrolyte* anion should also result in a differential stabilization of the solvation shell of the ion building the crystal depending on the background electrolyte used to adjust the ionic strength. Although all the electrolytes tested here are monovalent salts, the effective charge of the cations and anions in the background electrolyte is likely to be reduced as a consequence of the tendency of ions to pair in solution. When two ions in solution approach one another, their combined electric fields are significantly screened and, consequently, their electrostatic influence on hydration water and the stabilization is expected to diminish. Highly paired background ions should have a smaller effective charge and thus they would induce less stabilization in the water molecules of the calcium solvation shell than less paired salts (Ruiz-Agudo et al., 2010, 2011a,b). The net effect would be an increase in gypsum dissolution rate in the presence of highly paired salts compared to less paired salts.

Available experimental techniques in our laboratory cannot directly determine the arrangement of water molecules in the vicinity of a solvated ion. For this reason, we inferred the effect of background electrolyte ions from thermodynamic data. Under the conditions of low ionic strength used in our experiments, we use *the ionic surface tension increment of the background ion*, $k_i = d\gamma/d_{Cl}$ as a proxy for the effects of background ions on the solvation shell of ions building the crystal. Most salts in aqueous solutions increase the solution surface tension. These increments by aqueous electrolytes can be split into the contributions of the individual ions i of the electrolyte, k_i (i.e. the ionic surface tension increments) (Marcus, 2012). This parameter shows distinct dependencies for cations and anions, but an overall good linear inverse correlation with ionic size (Marcus, 2012). Moreover, it increases with net charge of the ion. Therefore, k_i increases with the solvation energies of the background electrolyte ions, and is expected to reflect the electrostatic interactions of background electrolytes on water of solvation of building ions, in a single parameter.

This idea is corroborated in our study considering the good correlation found between the different kinetic parameters obtained (both in macroscopic and, particularly, AFM dissolution experiments) and the ionic surface tension increments of the background electrolyte ions (Figs. 4 and 5). The higher the value of k_i, the smaller the ion and the higher its net effective charge; this would mean a strong interaction with the hydrated calcium ion and an enhanced stabilization of its water solvation shell. As explained in Section 4.2, this would result in slower dissolution rates, as we observed indeed in our experiments. Due to the uncertainties in the actual reactive surface area of the solids, kinetic parameters determined from AFM measurements (etch pit spreading rates and the volumetric acceleration per unit height) are regarded to be more accurate and representative of the actual dissolution rates.

The observed correlation of gypsum dissolution rates with k_i provide indirect evidence that support our hypothesis of the electrostatic interactions dictating the effect of the background electrolytes on the kinetics of gypsum dissolution. Interestingly, the dissolution rate was found to be higher in NO_3^- bearing solutions than in Cl^- solutions, opposite (as expected) to the trend observed by Bosbach et al. (1996) for gypsum growth, this supporting the validity of our model for gypsum growth as well.

5. CONCLUSIONS

The results of our micro- and macroscopic dissolution experiments, performed under conditions of constant, low ionic strength (0.05) and undersaturation (−0.045), provide experimental evidence for gypsum dissolution rates being ultimately controlled by the influence of the background salts on the hydration shell of the calcium ions. Dissolution

rates are systematically lower in the presence of 1:1 background electrolytes than in an electrolyte-free solution, regardless of the nature of the electrolyte tested. This can be explained considering that the presence of background ions electrostatically stabilizes the hydration shell of calcium. This has a direct entropic effect that reduces the overall ΔG of the system, so that dissolution is energetically less favorable. The correlation of dissolution rates with the ionic surface tension increments of the background electrolyte constituents further supports the validity of such a model for explaining the differential effect of electrolytes on gypsum dissolution. Our results are expected to contribute to a better understanding of how ions influence gypsum dissolution reactions, that may be of importance for a wide range of processes including the weathering of gypsum karst formations, deformation of gypsum-bearing rocks, the quality of drinking water, amelioration of soil acidity, scale formation in the oil and gas industry and solution creep of gypsum plasters. Furthermore, they are critical for the correct implementation of gypsum dissolution rate laws in the formulation of codes aimed at quantifying the kinetics of the natural and technologically relevant processes described above. This ultimately extends our ability to predict gypsum reactivity in the fluids of both engineering and natural systems.

ACKNOWLEDGMENTS

This research was done within the grants MAT2012-37584 and P11-RNM-7550, funded by the Spanish Government, European Commission (ERDF funds) and the Junta de Andalucía. ER-A acknowledges the receipt of a Ramón y Cajal grant from the Spanish Government (Ministerio de Economia y Competitividad) and funding from the research group RNM-179 of the Junta de Andalucía. The authors thank Veronika Rapelius for help with the ICP-OES analyses and Aurelia Ibañez-Velasco for assistant during dissolution experiments. CVP acknowledges funding from the EU through the Marie Curie initial training networks, MINSC and CO_2 React.

APPENDIX 1

As an approximation to global dissolution rates from AFM measurements, we used volumetric acceleration per height, a_v/h, which is time-independent and only depends on the etch pit spreading rates in a and b directions. It is defined according to:

$$\frac{dV}{dt} = \frac{d(a \cdot b \cdot sen(\alpha) \cdot h)}{dt} = h \cdot sen(\alpha) \cdot \frac{d(a \cdot b)}{dt} = h \cdot sen(\alpha) \cdot \left(\frac{b \cdot da + a \cdot db}{dt}\right) \quad \text{(A1)}$$

$$v_a = \frac{da}{dt} \text{ and } v_b = \frac{db}{dt} \quad \text{(A2)}$$

$$a = v_a \cdot t + a_0 \text{ and } b = v_b \cdot t + b_0 \quad \text{(A3)}$$

where a and b are the length of the etch pits measured by AFM, v_a and v_b the measured etch pits retreat velocities, h the height of the etch pits, α the angle between the directions [0 0 1](a) and [1 0 1](b) and V the empty volume of the etch pits.

Assuming that for a given pit h is constant in a short time sequence and the boundary conditions:

$$\text{if } t = 0 \text{ then } a_0 = b_0 = 0 \quad \text{(A4)}$$

$$\frac{dV}{dt} = 2 \cdot h \cdot \sin(\alpha) \cdot v_a \cdot v_b \cdot t \quad \text{(A5)}$$

$$V = h \cdot \sin(\alpha) \cdot v_a \cdot v_b \cdot t^2 \quad \text{(A6)}$$

Finally results:

$$a_V/h = \frac{d^2V}{h \cdot dt^2} = 2 \cdot \sin(\alpha) \cdot v_a \cdot v_b. \quad \text{(A7)}$$

APPENDIX 2

Plots showing the time evolution of the solution (left) free calcium concentration (mM) and (right) pH, during gypsum dissolution in an undersaturated solution (SI = −0.045) dosed with NH_4Cl (IS = 0.05).

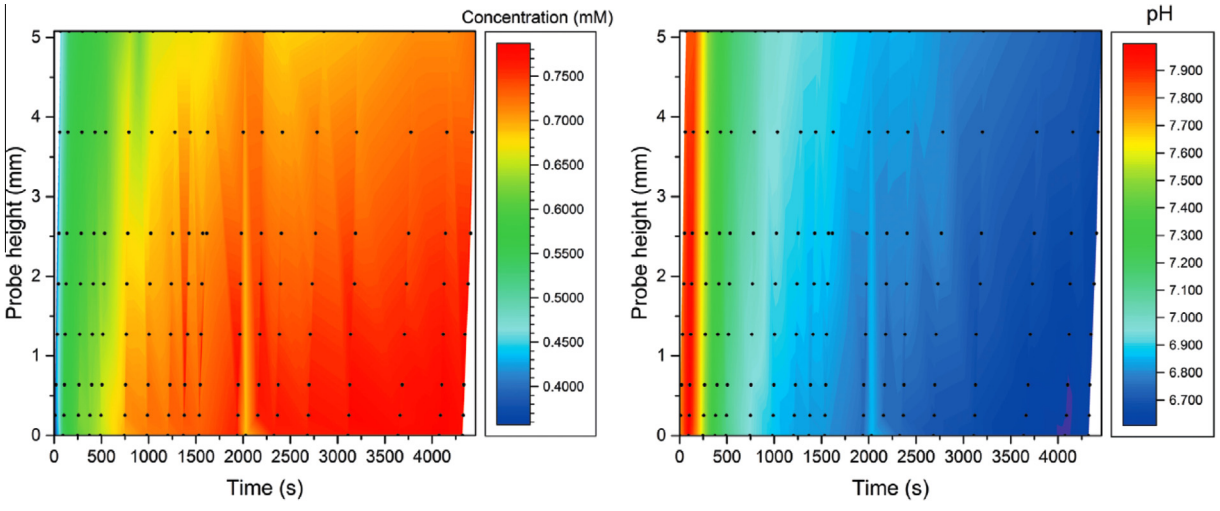

REFERENCES

Brandse W. P., van Rosmalen G. M. and Brouwer G. (1977) The influence of sodium chloride on the crystallization rate of gypsum. *J. Inorg. Nucl. Chem.* **39**, 2007–2010. http://dx.doi.org/10.1016/0022-1902(77)80534-4.

Buhmann D. and Dreybrodt W. (1987) Calcite dissolution kinetics in the system H_2O–CO_2–$CaCO_3$ with participation of foreign ions. *Chem. Geol.* **64**, 89–102. http://dx.doi.org/10.1016/0009-2541(87)90154-9.

Bosbach D. and Rammensee W. (1994) In situ investigation of growth and dissolution on the (0 1 0) surface of gypsum by Scanning Force Microscopy. *Geochim. Cosmochim. Acta* **58**, 843–849. http://dx.doi.org/10.1016/0016-7037(94)90509-6.

Bosbach D., Junta-Rosso J. L., Becker U. and Hochella M. F. (1996) Gypsum growth in the presence of background electrolytes studied by scanning force microscopy. *Geochim. Cosmochim. Acta* **60**, 3295–3304. http://dx.doi.org/10.1016/0016-7037(96)00147-0.

Bracco J. N., Grantham M. G. and Stack A. G. (2012) Calcite growth rates as a function of aqueous calcium-to-carbonate ratio, saturation index, and inhibitor concentration: insight into the mechanism of reaction and poisoning by strontium. *Cryst. Growth Des.* **12**, 3540–3548. http://dx.doi.org/10.1021/cg300350k.

Bracco J. N., Stack A. G. and Higgins S. R. (2014) Magnesite step growth rates as a function of the aqueous magnesium: carbonate ratio. *Cryst. Growth Des.* **14**, 6033–6040. http://dx.doi.org/10.1021/cg501203g.

Chen J. and Jiang M. (2009) Long-term evolution of delayed ettringite and gypsum in Portland cement mortars under sulfate erosion. *Constr. Build. Mater.* **23**, 812–816. http://dx.doi.org/10.1016/j.conbuildmat.2008.03.002.

Colombani J. and Bert J. (2007) Holographic interferometry study of the dissolution and diffusion of gypsum in water. *Geochim. Cosmochim. Acta* **71**, 1913–1920. http://dx.doi.org/10.1016/j.gca.2007.01.012.

De Meer S. and Spiers C. J. (1997) Uniaxial compaction creep of wet gypsum aggregates. *J. Geophys. Res.* **102**, 875. http://dx.doi.org/10.1029/96JB02481.

De Yoreo J. J. and Vekilov P. G. (2003) Principles of crystal nucleation and growth. *Rev. Mineral. Geochem.* **54**, 57.

Dove P. M. and Czank C. a. (1995) Crystal chemical controls on the dissolution kinetics of the isostructural sulfates: celestite, anglesite, and barite. *Geochim. Cosmochim. Acta* **59**, 1907–1915. http://dx.doi.org/10.1016/0016-7037(95)00116-6.

Fan C. and Teng H. H. (2007) Surface behavior of gypsum during dissolution. *Chem. Geol.* **245**, 242–253. http://dx.doi.org/10.1016/j.chemgeo.2007.08.007.

Fischer C., Arvidson R. S. and Lüttge A. (2012) How predictable are dissolution rates of crystalline material? *Geochim. Cosmochim. Acta* **98**, 177–185. http://dx.doi.org/10.1016/j.gca.2012.09.011.

Hall C. and Cullen D. C. (1996) Scanning force microscopy of gypsum dissolution and crystal growth. *AIChE J.* **42**, 232–238. http://dx.doi.org/10.1002/aic.690420119.

Jeschke A. A., Vosbeck K. and Dreybrodt W. (2001) Surface controlled dissolution rates of gypsum in aqueous in solutions exhibit nonlinear dissolution kinetics. *Geochim. Cosmochim. Acta* **65**, 27–34. http://dx.doi.org/10.1016/S0016-7037(00)00510-X.

Jordan G. and Rammensee W. (1998) Dissolution rates of calcite obtained by scanning force microscopy: microtopography-based dissolution kinetics on surfaces with anisotropic step velocities. *Geochim. Cosmochim. Acta* **62**, 941–947. http://dx.doi.org/10.1016/S0016-7037(98)00030-1.

Koneshan S., Rasaiah J. C., Lynden-Bell R. M. and Lee S. H. (1998) Solvent structure, dynamics, and ion mobility in aqueous solutions at 25 °C. *J. Phys. Chem. B* **102**, 4193–4204. http://dx.doi.org/10.1021/jp980642x.

Kowacz M. and Putnis A. (2008) The effect of specific background electrolytes on water structure and solute hydration: consequences for crystal dissolution and growth. *Geochim. Cosmochim. Acta* **72**, 4476–4487. http://dx.doi.org/10.1016/j.gca.2008.07.005.

Kowacz M., Putnis C. V. and Putnis A. (2007) The effect of cation: anion ratio in solution on the mechanism of barite growth at constant supersaturation: role of the desolvation process on the growth kinetics. *Geochim. Cosmochim. Acta* **71**, 5168–5179.

Kuechler R., Noack K. and Zorn T. (2004) Investigation of gypsum dissolution under saturated and unsaturated water conditions. *Ecol. Modell.* **176**, 1–14. http://dx.doi.org/10.1016/j.ecolmodel.2003.10.025.

Liang Y., Baer D. R., McCoy J. M. and Amonette J. E. (1996) Dissolution kinetics at the calcite–water interface. *Geochim. Cosmochim. Acta* **60**, 4883–4887. http://dx.doi.org/10.1016/S0016-7037(96)00337-7.

Luttge A., Arvidson R. S. and Fischer C. (2013) A stochastic treatment of crystal dissolution kinetics. *Elements* **9**, 183–188. http://dx.doi.org/10.2113/gselements.9.3.183.

Marcus Y. (2012) *Ions in Water and Biophysical Implications*. Springer, London, http://doi.org/10.1007%2F978-94-007-4647-3.

Pachon-Rodriguez E. A., Guillon E., Houvenaghel G. and Colombani J. (2011) Pressure solution as origin of the humid creep of a mineral material. *Phys. Rev. E Stat. Nonlin. Soft Matter Phys.* **84**. http://dx.doi.org/10.1103/PhysRevE.84.066121.

Perdikouri C., Putnis C. V., Kasioptas A. and Putnis A. (2009) An atomic force microscopy study of the growth of a calcite surface as a function of calcium/total carbonate concentration ratio in solution at constant supersaturation. *Cryst. Growth Des.* **9**, 4344–4350. http://dx.doi.org/10.1021/cg900200s.

Pokrovsky O. S. and Schott J. (2002) Surface chemistry and dissolution kinetics of divalent metal carbonates. *Environ. Sci. Technol.* **36**, 426–432. http://dx.doi.org/10.1021/es010925u.

Raines M. and Dewers T. (1997) Mixed transport/reaction control of gypsum dissolution kinetics in aqueous solutions and initiation of gypsum karst. *Chem. Geol.* **140**, 29–48. http://dx.doi.org/10.1016/S0009-2541(97)00018-1.

Raju K. U. G. and Atkinson G. (1990) The thermodynamics of "scale" mineral solubilities. 3. Calcium sulfate in aqueous sodium chloride. *J. Chem. Eng. Data* **35**, 361–367. http://dx.doi.org/10.1021/je00061a038.

Ruiz-Agudo E. and Putnis C. V. (2012) Direct observations of mineral fluid reactions using atomic force microscopy: the specific example of calcite. *Mineral. Mag.* **76**, 227–253. http://dx.doi.org/10.1180/minmag.2012.076.1.227.

Ruiz-Agudo E., Kowacz M., Putnis C. V. and Putnis a. (2010) The role of background electrolytes on the kinetics and mechanism of calcite dissolution. *Geochim. Cosmochim. Acta* **74**, 1256–1267. http://dx.doi.org/10.1016/j.gca.2009.11.004.

Ruiz-Agudo E., Putnis C. V., Wang L. and Putnis A. (2011a) Specific effects of background electrolytes on the kinetics of step propagation during calcite growth. *Geochim. Cosmochim. Acta* **75**, 3803–3814. http://dx.doi.org/10.1016/j.gca.2011.04.012.

Ruiz-Agudo E., Urosevic M., Putnis C. V., Rodríguez-Navarro C., Cardell C. and Putnis A. (2011b) Ion-specific effects on the kinetics of mineral dissolution. *Chem. Geol.* **281**, 364–371. http://dx.doi.org/10.1016/j.chemgeo.2011.01.003.

Samoilov O. Y. (1967a) The theory of salting out from aqueous solutions – I. General problems. *J. Struct. Chem.* **7**, 12–19. http://dx.doi.org/10.1007/BF00739228.

Samoilov O. Y. (1967b) The theory of the salting out in aqueous solutions – II. Dependence of dehydration and hydration on the initial degree of hydration of a cation undergoing salting out. *J. Struct. Chem.* **7**, 177–180. http://dx.doi.org/10.1007/BF00744285.

Samoilov O. Y. (1971) Theory of salting out from aqueous solutions – III. Dependence of salting out on characteristics of ions of salting-out agent. *J. Struct. Chem.* **11**, 929–931. http://dx.doi.org/10.1007/BF00744583.

Schmid R., Miah A. M. and Sapunov V. N. (2000) A new table of the thermodynamic quantities of ionic hydration: values and some applications (enthalpy–entropy compensation and Born radii). *Phys. Chem. Chem. Phys.* **2**, 97–102. http://dx.doi.org/10.1039/a907160a.

Sumner M. E., Shahandeh H., Bouton J. and Hammel J. (1986) Amelioration of an acid soil profile through deep liming and surface application of gypsum. *Soil Sci. Soc. Am. J.* **50**. http://dx.doi.org/10.2136/sssaj1986.03615995005000050069x (NP).

Stack A. G. and Grantham M. C. (2010) Growth rate of calcite steps as a function of aqueous calcium-to-carbonate ratio: independent attachment and detachment of calcium and carbonate ions. *Cryst. Growth Des.* **10**, 1409–1413.

Weijnen M. P. C., van Rosmalen G. M., Bennema P. and Rijpkema J. J. M. (1987) Tjushe adsorption of additives at the gypsum crystal surface: a theoretical approach. *J. Cryst. Growth* **82**, 528–542. http://dx.doi.org/10.1016/0022-0248(87)90345-9.

Wolthers M., Nehrke G., Gustafsson J. P. and Van Cappellen P. (2012) Calcite growth kinetics: modeling the effect of solution stoichiometry. *Geochim. Cosmochim. Acta* **77**, 121–134. http://dx.doi.org/10.1016/j.gca.2011.11.003.

Wolthers M., Putnis C. V. and Ruiz-Agudo E. (2015) Calcite dissolution kinetics and mechanism depend on solution stoichiometry. In *Goldschmidt Abstracts*, p. 3439.

Associate editor: Carl Steefel